

RESEARCH ARTICLE

A tree-ring $\delta^{18}\text{O}$ based reconstruction of East Asia summer monsoon over the past two centuries

Dai Chen¹✉, Feifei Zhou²✉, Zhipeng Dong², A'ying Zeng², Tinghai Ou³, Keyan Fang^{2,3*}

1 National Forestry and Grassland Administration, National Park Administration, Beijing, China, **2** Key Laboratory of Humid Subtropical Eco-geographical Process, Ministry of Education, College of Geographical Sciences, Fujian Normal University, Fuzhou, China, **3** Department of Earth Sciences, Regional Climate Group, University of Gothenburg, Gothenburg, Sweden

✉ These authors contributed equally to this work.

* kfang@fjnu.edu.cn



OPEN ACCESS

Citation: Chen D, Zhou F, Dong Z, Zeng A, Ou T, Fang K (2020) A tree-ring $\delta^{18}\text{O}$ based reconstruction of East Asia summer monsoon over the past two centuries. PLoS ONE 15(6): e0234421. <https://doi.org/10.1371/journal.pone.0234421>

Editor: Caroline Ummenhofer, Woods Hole Oceanographic Institution, UNITED STATES

Received: October 1, 2019

Accepted: May 26, 2020

Published: June 9, 2020

Copyright: © 2020 Chen et al. This is an open access article distributed under the terms of the [Creative Commons Attribution License](https://creativecommons.org/licenses/by/4.0/), which permits unrestricted use, distribution, and reproduction in any medium, provided the original author and source are credited.

Data Availability Statement: All relevant data are within the Supporting Information files.

Funding: This research is funded by the National Science Foundation of China (41888101, 41822101, 41971022 and 41772180) to KF (<http://www.nsf.gov.cn/>), the Strategic Priority Research Program of the Chinese Academy of Sciences (XDB26020000) to KF (<http://www.cas.cn/kxyj/ky/index.shtml#xdzx>), the Natural Science Foundation Project of Fujian Province (2017J0101) to FZ (<http://www.cma.gov.cn/>), fellowship for the

Abstract

The East Asian summer monsoon (EASM) exhibits considerable decadal variations since the late 20th century. Efforts to examine long-term behaviors and dynamics of the EASM are impeded largely due to the shortness of instrumental meteorological records. So far, reconstructions of the EASM with annual resolution from its core regions remain limited. We conduct the first 200-year robust EASM reconstruction based on tree-ring cellulose $\delta^{18}\text{O}$ records derived from *Pinus massoniana* trees growing in the middle Yangtze River basin, one of the core EASM areas. The $\delta^{18}\text{O}$ chronology accounts for 46.2% of the actual variation in an index of the EASM from 1948 to 2014. The reconstructed EASM indicates that the monsoon intensity was below average before the 1950s, peaked in the 1950s-1970s, and then began to decline. The reconstructed EASM is negatively correlated with the El Niño-Southern Oscillation (ENSO), but this teleconnection is dynamic through time, i.e. enhanced (reduced) ENSO variability coheres with strong (weak) EASM-ENSO connections. In addition, despite high ENSO variability since the 1980s, the EASM-ENSO relationship weakened possibly due to anthropogenic impact, particularly aerosol emissions.

Introduction

The Asian summer monsoon is the strongest monsoon system on Earth, influencing the hydroclimatic conditions of dozens of countries and livelihood of roughly half of the world's population [1, 2]. The East Asian summer monsoon (EASM) is a subtropical monsoon encompassing East China, Japan and Korea [3, 4]. EASM reaches the northernmost location in the global monsoon system to semi-arid regions in eastern and central Asia, forming the ecotone between agricultural and animal husbandry. Abrupt shifts of EASM usually lead to anomalous hydroclimate changes in East Asia with devastating consequences for regional agriculture and socioeconomics [1, 5] and even alternation of dynasties in history [6, 7].

National Youth Talent Support Program of China (Ten Thousand People Plan) to KF (<http://rencai.people.com.cn/>), and a fellowship for Youth Talent Support Program of Fujian Province and the innovation team project (IRTL1705) to KF (<http://rencai.people.com.cn/>). This research is also funded by the Swedish Formas and VR projects (<https://www.formas.se/en/>).

Competing interests: The authors have declared that no competing interests exist.

Proxy-based reconstructions of EASM have revealed positive responses of EASM to historical warming at centennial- or even millennial-long scales [8, 9]. However, under the recent global warming, the instrumental records indicated a decay of EASM [1, 10, 11]. It is generally believed that recent changes in EASM is strongly influenced by enhanced anthropogenic forcings [1, 10]. To evaluate the recent anomaly, a long-term background of natural EASM variability is needed. Although there have been some EASM reconstructions from lake sediments [9, 12], peat deposits [13] and stalagmites [8, 14], these archives are often unable to resolve interannual to interdecadal variations due to dating accuracy and coarse sampling resolution. This poses a challenge in deriving a robust calibration with the EASM index, hence high-resolution proxy records are needed.

Tree rings can provide exactly dated, annually resolved information about past climates [15, 16]. A growing body of tree-ring chronologies were published from the core areas of the EASM-affected regions (e.g. South and East China) [17, 18, 19, 20], but seldom were used to reflect EASM dynamics because tree rings in these warm and humid conditions are normally insensitive to hydroclimate changes [21]. Tree-ring cellulose oxygen isotopes ($\delta^{18}\text{O}$) usually contain information on source water isotope compositions and atmospheric vapor pressure deficit [22], which are closely related to regional precipitation $\delta^{18}\text{O}$ [23]. Precipitation $\delta^{18}\text{O}$ is negatively correlated with precipitation amounts due to the “amount effect” in the tropical monsoon environment [24, 25, 26, 27]. Therefore, oxygen isotope records preserved in tree-ring cellulose are potential archives of robust monsoonal hydroclimate signals in many warm-humid regions [28, 29, 30, 31, 32]. Moreover, the tree-ring $\delta^{18}\text{O}$ preserve long-term climate trends, since it does not require trend removal, in contrast to tree-ring width data.

In this study, we built a $\delta^{18}\text{O}$ chronology from *Pinus massoniana* trees in the middle Yangtze River basin, a core area of EASM [33], to derive the first reconstruction of EASM index covering the period from 1815 to 2014. Based on this reconstruction, we investigate the characteristics and regimes of EASM with a long-term perspective and identified possible processes that drive EASM over the past two centuries.

Material and methods

Ethics statement

All field work and sampling were carried out with official permission from Hubei and Hunan Forestry Bureau, China.

Climate and tree-ring width data

The sampling sites (HP, 110.55° E, 30° N, 860m a.s.l.; WL, 110.67° E, 29.83° N, 893m a.s.l.), located in the middle Yangtze River basin, have a humid and warm subtropical monsoon climate (Table 1; Fig 1A). The instrumental records from the nearest Shimen meteorological station (111.37° E, 29.58° N, 198 m a.s.l.), obtained from China Meteorological Administration (www.nmic.gov.cn), reveal that the mean annual total rainfall from 1960 to 2014 is 1360 mm, the annual average temperature is 16.9°C and the mean relative humidity is 75.4% during the period of 1961–2016. The average total precipitation in monsoonal season (June–July–August) exceeds 580 mm, contributing more than 42% of the annual total precipitation. The monsoonal precipitation shows strong interannual variability, with the standard deviation exceeding 210 mm.

The EASM index (Fig 1B) used as a calibration data for reconstruction is defined as an area-averaged seasonally (June–July–August) [dynamical normalized seasonality](#) of wind fields at 850 hPa within the East Asian monsoon domain (10°–45° N, 110°–140° E) during the 1948–2014 period [33]. The index is available from the website (<http://ljpgcscn/dct/page/65577>),

Table 1. Statistics of the two tree-ring sampling sites, the Shimen meteorological station and the CRU grid point.

Data type	Site code	Location (Longitude, latitude)	Elevation (m)	Number (core/tree)
Tree-ring	HPS	110.55° E, 30° N	860	36/18
	WL	110.67° E, 29.83° N	893	30/15
Meteorological data	Shimen	111.37° E, 29.58° N	198	

<https://doi.org/10.1371/journal.pone.0234421.t001>

which is widely used to show summer monsoon activity in the middle-lower Yangtze River basin [33]. In addition, monthly gridded precipitation from the Climate Research Unit (CRU) TS4.03 [34] and monthly sea surface temperatures (SSTs) during 1870–2014 from the Hadley Centre Sea Ice and Sea Surface Temperature dataset version 1.1 (HadISST1.1) [35] are used for climate-proxy relationship analysis. The spatial correlations between the EASM index and SSTs are used to investigate the teleconnections between EASM and large-scale atmospheric-oceanic circulations. The spatial correlation analysis are performed using the KNMI Climate Explorer (<http://www.knmi.nl>), a web-based application for [high-resolution paleoclimatology](#) [36].

In the fieldwork, two cores per tree were extracted using increment borers. In total, 66 increment cores were taken from 33 living *P. massoniana* trees at the sites (Table 1). The samples were mounted, air dried, polished and cross-dated based on the standard dendrochronology procedures [37, 38]. Ring widths were measured to 000.1 mm accuracy and quality checked with moving correlations using the COFECHA program [39]. The ARSTAN program [40] was used for the standard chronology development. As the sample size generally declines in the early portion of a tree-ring chronology, the subsample signal strength (SSS) statistic [41] with a threshold value of 0.85 is employed to evaluate the most reliable time span of the chronology. The final ring-width chronology exceeds the SSS threshold of 0.85 over the period 1815 to 2014 (S2 Fig).

Cellulose extraction and oxygen isotope measurements

We selected eight cores from eight trees (5 cores from HP, 3 cores from WL) with no absent rings and homogeneous growth patterns (interseries correlations greater than 0.5) for stable isotopes analysis, covering a period of 1815–2014. We “pool” the whole wood from their annual rings prior to α -cellulose extraction following standard pooling methodology [42]. The “pooling” method has been proven to be reliable at our sites according to high coherency of tree-ring cellulose $\delta^{18}\text{O}$ data of four individual cores from four different trees during the period of 1950–2014 (S3 Fig and S1 Table). Then α -cellulose of the annual tree rings were extracted following a modified method of [43] and [44]. In order to homogenize the cellulose, an ultrasonic water bath (JY92-2D, Scientz Industry, Ningbo, China) was used to break the cellulose fibers. The α -cellulose was then freeze-dried for three days prior to isotope analysis. The tree-ring $\delta^{18}\text{O}$ values were measured using a High Temperature Conversion Elemental Analyzer (TC/EA) coupled to a Finnigan MAT-253 mass spectrometer (Thermo Electron Corporation, Bremen, Germany). Each cellulose sample was repeatedly measured four times to improve precision. The resulting standard deviation of the replicates was less than 0.3‰ based on the four measurements [24]. We calculated the mean isotopic values of each sample without outliers (values more than three standard deviations from the mean). We measured the ratio for a benzoic acid working standard (repeated four times) with a known $\delta^{18}\text{O}$ value (IAEA-601, 23.3‰) every seven measurements to monitor the analytical precision and to calibrate the samples for analytical accuracy [45]. The IAEA-C3 cellulose standard ($\delta^{18}\text{O} = 3.22\text{‰}$) was also

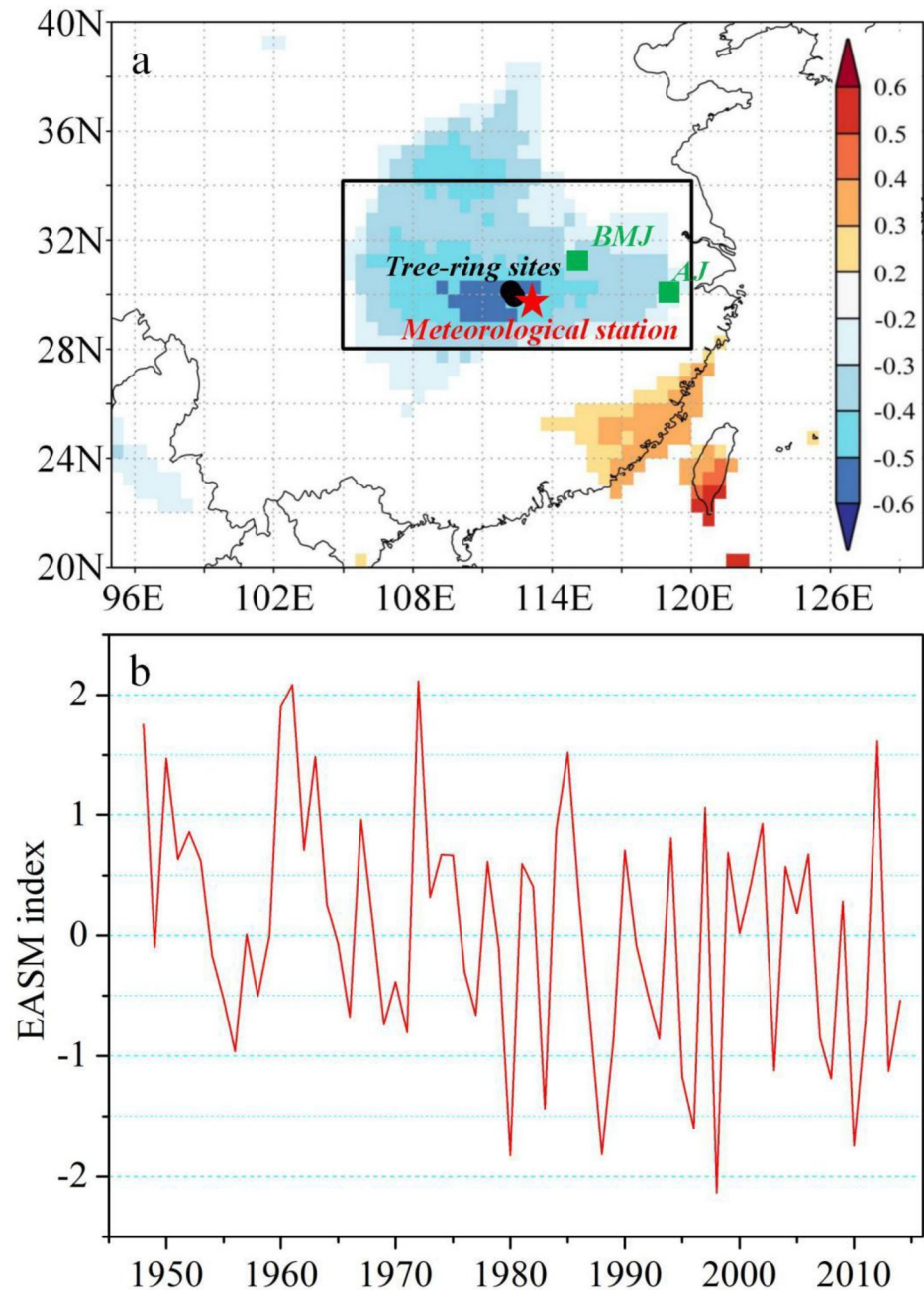


Fig 1. (a) Locations of the tree-ring sampling sites (circle), the meteorological station (star) and the other tree-ring $\delta^{18}\text{O}$ based precipitation reconstructions (square) [30, 31]; background colors represent the spatial correlations between the observed EASM index [33] and CRU TS4.03 precipitation (from June to August); the black box highlights the study area; (b) The observed EASM index from 1948 to 2014.

<https://doi.org/10.1371/journal.pone.0234421.g001>

employed here to calibrate the tree-ring oxygen measurements. The resulting standard deviation of the replicates was less than 0.3‰ based on four measurements.

EASM reconstruction

EASM reconstruction was conducted by a simple linear regression model on the basis of a split calibration-verification procedure that was designed to test the model reliability [46]. A

number of statistics were employed to evaluate model ability, including simple correlation coefficient (R), R square (R^2), reduction of error (RE) and coefficient of efficiency (CE). Values of RE and CE greater than zero indicate rigorous model skill [16].

Results

Significant spatial correlations are found between the EASM index and summer precipitation from CRU TS4.03 in the middle-lower valleys of Yangtze River (Fig 1A), indicating that the tree-ring sites are located in the core regions of EASM. The composite tree ring $\delta^{18}\text{O}$ chronology from *P. massoniana* trees at our sites is given in Fig 2. The mean and standard deviation of the $\delta^{18}\text{O}$ time series are 26.19‰ and 0.99‰, respectively. The autocorrelation (one year lag) of the $\delta^{18}\text{O}$ chronology is 0.15. Correlation analysis was performed between the tree-ring $\delta^{18}\text{O}$ chronology and monthly climate variables (temperature, precipitation and relative humidity) from previous November to current October during the period of 1960–2014. The $\delta^{18}\text{O}$ signatures correlated significantly ($P < 0.05$, $N = 55$) and negatively with precipitation and relative humidity from May to August (Fig 3A). In addition, tree-ring cellulose $\delta^{18}\text{O}$ records also show significant ($P < 0.05$, $N = 55$) and positive correlations with temperature during the months of June, July and August. It appears that the hydroclimatic changes during the monsoonal season are the dominant limitations for tree-ring $\delta^{18}\text{O}$ in the study area. The highest correlation (0.67, $P < 0.01$, $N = 55$) with climate is observed for precipitation in the combined months from May to August.

Given close associations of tree-ring $\delta^{18}\text{O}$ with summer monsoon rainfall, the correlation with the EASM index [33] was calculated for the 1948–2014 period. The high correlation (0.68, $p < 0.001$, $N = 67$) between the EASM index and tree-ring $\delta^{18}\text{O}$ indicates that the EASM index can be a strong predictand of variance in tree-ring $\delta^{18}\text{O}$ in the study area (Fig 3B), and was selected as the target for reconstruction. The linear regression model accounts for 46.2% of the actual variance of EASM during 1948–2014. As shown in Table 2, the calibration and verification results for the split subperiods, i.e. 1948–1980 and 1981–2014, generally show a good model fit. Based on this model we reconstruct temporal changes of EASM for the past 200 years (Fig 4). Wavelet power spectrum analysis indicates that the reconstructed EASM contains interannual (<10 years) variations at a confidence level greater than 95% (S5 Fig).

Spatial correlations between the reconstructed EASM and global December-February SSTs show an El Niño-Southern Oscillation (ENSO) like pattern during the common period of 1870–2014 (Fig 5). However, based on the 31-year sliding correlations between the reconstructed EASM and the tree-ring-based ENSO reconstruction [47] during the common period of 1815–2005 (Fig 6A), the EASM-ENSO relationships broke down during the periods of 1830–1890 and 1930–1960 when the ENSO variance was low (Fig 6B).

Discussion

Climatic implications of tree-ring $\delta^{18}\text{O}$

Based on tree-ring cellulose isotope fractionation model, negative correlations are expected between tree-ring cellulose $\delta^{18}\text{O}$ and relative humidity [25]. Low relative humidity enhances vapor pressure gradients between leaf interstitial spaces and the atmosphere, which could cause the preferential loss of lighter isotope and enrich the oxygen isotopes in leaf water [25]. Lower humidity also increases the evaporation of soil water in the upper layer, thus the source water taken up by roots becomes heavier [29]. Similarly, high temperature normally causes enhanced evapotranspiration and decreased relative humidity levels. Therefore, positive correlations are observed between tree-ring cellulose $\delta^{18}\text{O}$ and temperature in the study area.

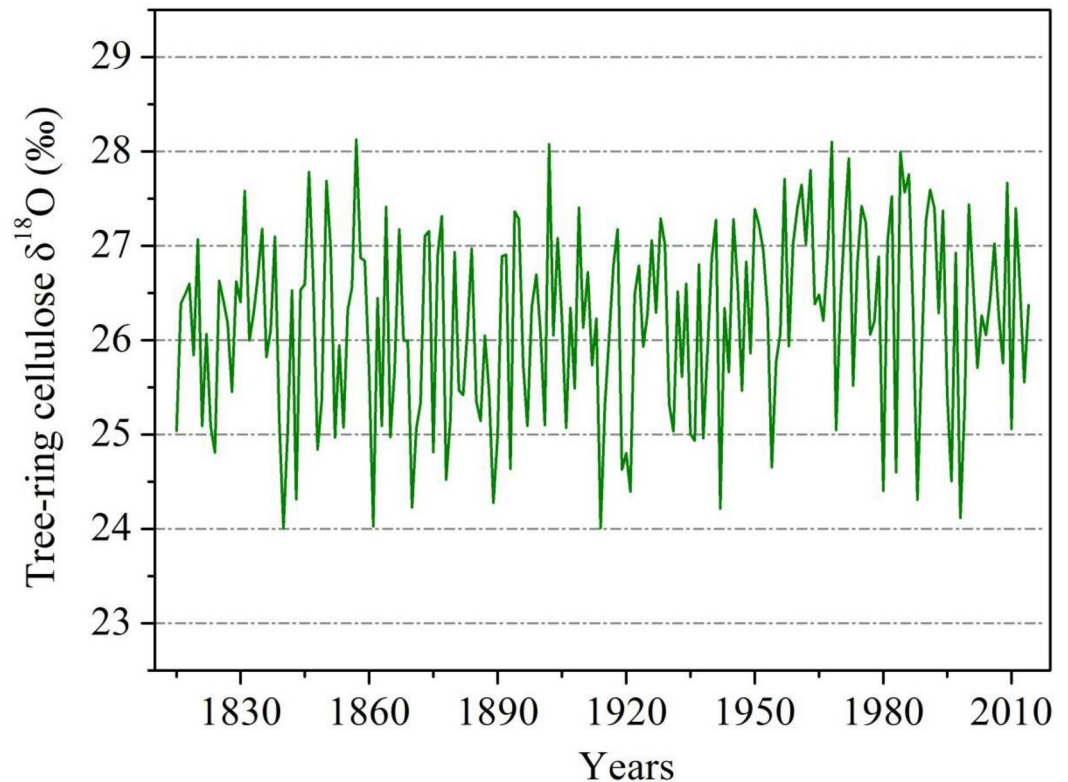


Fig 2. The tree-ring $\delta^{18}\text{O}$ chronology during the period 1815–2014.

<https://doi.org/10.1371/journal.pone.0234421.g002>

Negative relationships between precipitation and tree-ring cellulose $\delta^{18}\text{O}$ levels are reported frequently in monsoonal areas [28, 29, 30, 31]. Precipitation affects tree-ring cellulose $\delta^{18}\text{O}$ mainly via relative humidity and $\delta^{18}\text{O}$ in the precipitation itself. On one hand, more precipitation usually equals higher relative humidity during the monsoonal season in the study area (S4 Fig). On the other hand, due to the amount effect [24, 25], isotope-enriched water vapor is more easily removed by condensation due to the mass discrepancy between H_2^{18}O and H_2^{16}O , making the isotopic composition of the remaining vapor lighter [48]. The higher the amount of the precipitation totals, the more depleted is the isotopic composition of the water vapor. Therefore, greater precipitation is associated with higher relative humidity and more $\delta^{18}\text{O}$ depleted precipitation, leading to lower tree-ring cellulose $\delta^{18}\text{O}$.

Historical EASM variations

We used tree-ring $\delta^{18}\text{O}$ to reconstruct EASM variations based on the strong linear correlation between tree-ring $\delta^{18}\text{O}$ and the EASM index. The EASM reconstruction was compared with the tree-ring $\delta^{18}\text{O}$ based May-June precipitation reconstruction for Baimajian (BMJ, 31.12°N, 116.18°E) and May-October precipitation reconstruction for Anji (AJ, 30.39°N, 119.43°E) (Fig 1A) over the middle-lower Yangtze River basin, respectively [30, 31]. As shown in Fig 7, the reconstructed EASM and the two reconstructed precipitation records exhibit a high degree of coherency at interdecadal scales, with a significant negative correlation ($p < 0.05$) value of -0.56 with the BMJ for 1845–2011, and -0.48 with the AJ for 1870–2013. The correlations are significant ($p < 0.05$) after accounting for the effective degrees of freedom due to the low-pass filtering using the modified Chelton method [49, 50, 51]. In addition, many anomalous flooding events

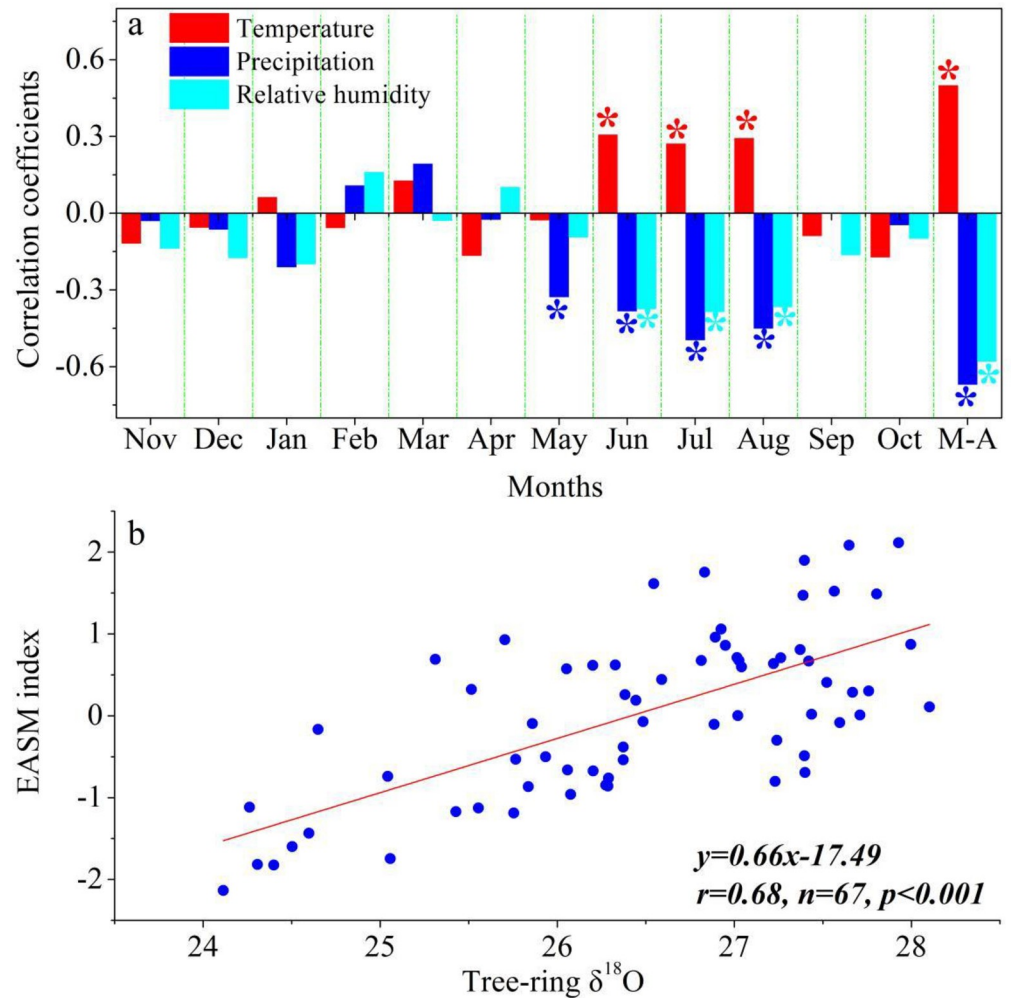


Fig 3. a) Correlations calculated between the tree-ring $\delta^{18}\text{O}$ chronology and climate variables recorded by Shanghang meteorological station from previous November to current October during the period of 1960–2014. M-A symbolizes the combined months from May to August. Stars indicate the 95% confidence level; b) Relationship between the $\delta^{18}\text{O}$ chronology and the observed EASM index for the period of 1948–2014.

<https://doi.org/10.1371/journal.pone.0234421.g003>

over the middle-lower reaches of Yangtze River recorded by historical documents [52] and grain-size variations of deposition from the subaqueous Yangtze River delta [53] are consistent with low extremes of the reconstructed EASM (S2 Table). These results here reinforce the robustness of the reconstruction model.

Table 2. Statistics of the split calibration-verification model for the EASM reconstruction.

	Calibration (1948–1980)	Verification (1981–2014)	Calibration (1981–2014)	Verification (1948–1980)	Full calibration (1948–2014)
R	0.66**	0.71**	0.71**	0.66**	0.69**
R ²					0.48
RE		0.44		0.52	
CE		0.49		0.39	

RE: reduction of error; CE: Coefficient of efficiency
 ** represents the the 99% confidence level

<https://doi.org/10.1371/journal.pone.0234421.t002>

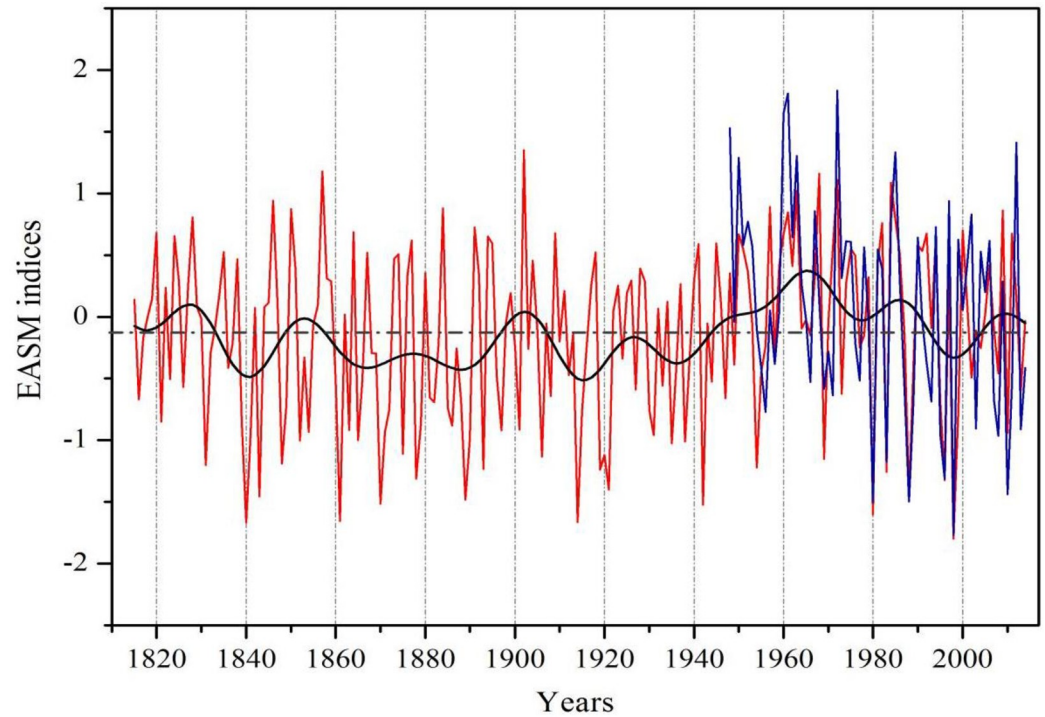


Fig 4. The EASM reconstruction (red line) back to 1815, with the interdecadal variations (bold black line) isolated by using a 20-year fast-Fourier transform filter and the target time series (blue line) for the 1948–2014 period of overlap. The horizontal dashed line represents the mean value of the reconstructed EASM over the period of 1815–2014.

<https://doi.org/10.1371/journal.pone.0234421.g004>

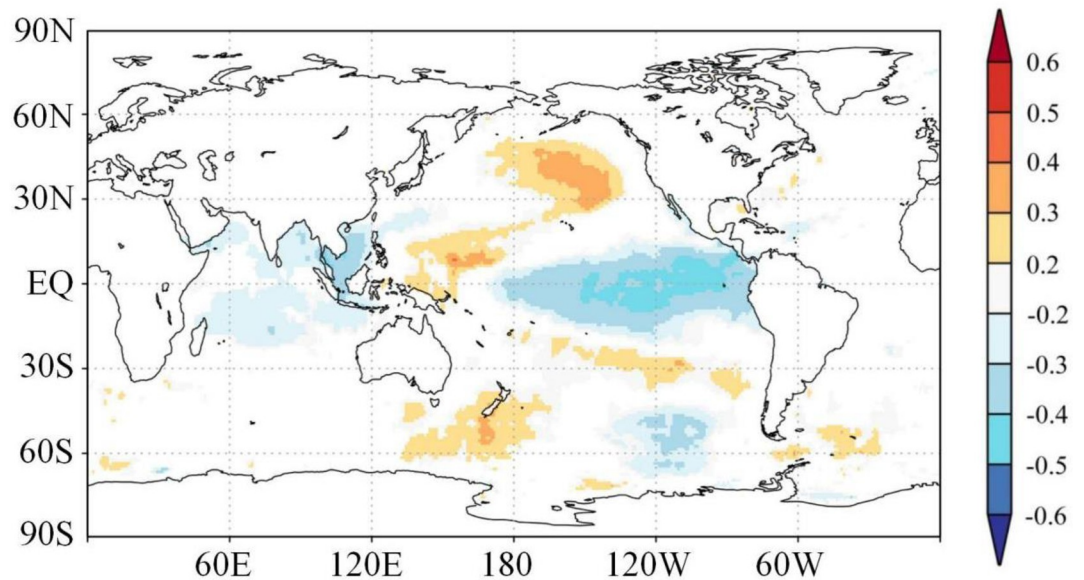


Fig 5. Correlations between the reconstructed EASM and precedent winter (from December to February) global SSTs for the period of 1871–2014. Correlations not significant at the 95% level have been masked out. The maps were produced with GrADS v2.2.0 software (<http://cola.gmu.edu/grads/>) in KNMI Climate Explorer.

<https://doi.org/10.1371/journal.pone.0234421.g005>

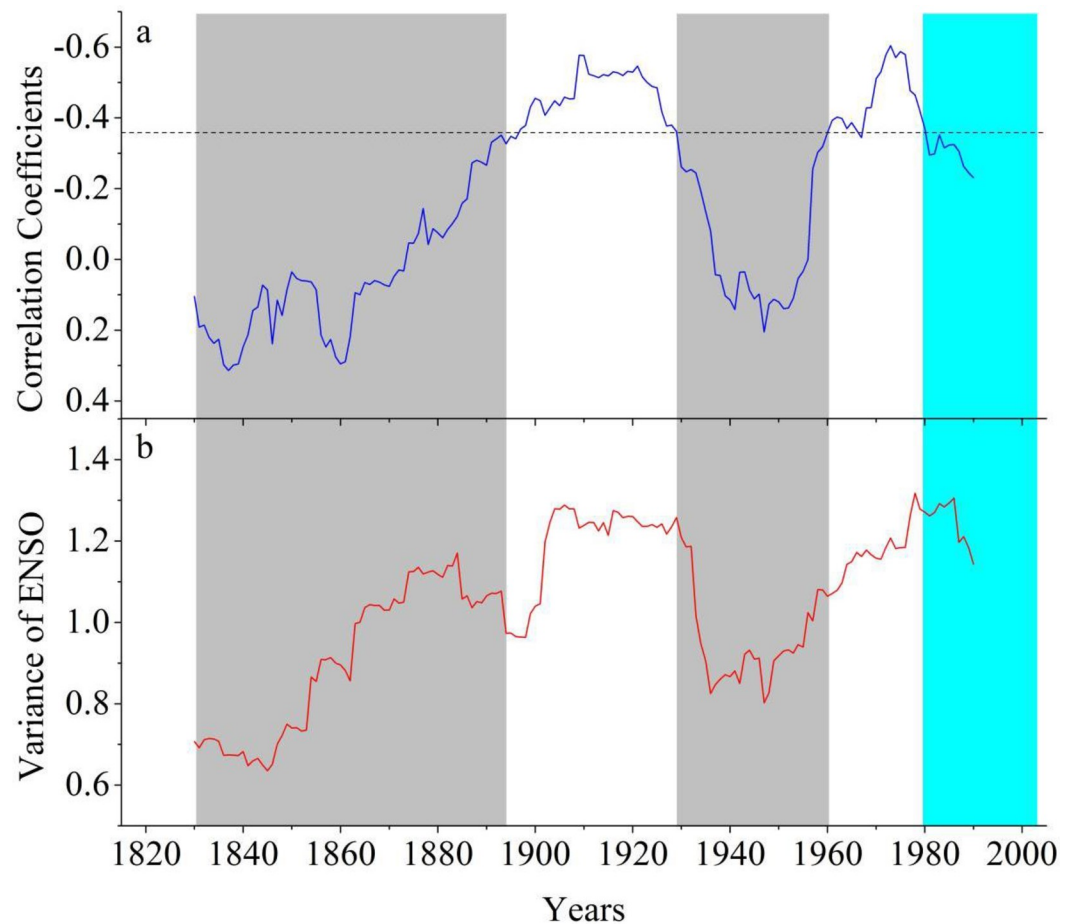


Fig 6. a) The 31-year running correlations (assigned to center year of the window) between the reconstructed EASM and the reconstructed ENSO variability [47] during the common period of 1815–2005. The dashed line symbolizes the 95% confidence level; b) The 31-year running variability of the reconstructed ENSO indices during the period of 1815–2005.

<https://doi.org/10.1371/journal.pone.0234421.g006>

The reconstructed EASM was generally low and fluctuated moderately in the 19th century, which coincided with the end of the Little Ice Age. In history, the decay of summer monsoon generally occurred during the periods of warmer temperature, and vice versa [1, 54, 55, 56]. More dramatic fluctuations were observed since the 20th century, and the most severe and long-lasting above-average EASM anomalies over the past two centuries occurred during the 1950s–1980s. The stronger EASM during this period may be associated with the increased thermal gradient between the Eurasian continent and the tropical oceans due to global warming, as suggested by a number of synoptic and modeling studies [57, 58, 59]. In addition, although concomitant with global warming, EASM has experienced a moderate decreasing tendency since the 1970s, which is consistent with analysis based on the instrumental data [60, 61]. Despite having mechanisms proposed for the recent weakening of EASM [62, 63, 64, 65], great uncertainties still exist [65]. Some studies attribute the current weakening of EASM to the enhancement of anthropogenic activities [61, 62], while others consider the impacts of natural processes such as oceanic and atmospheric modes [63, 64].

Links with large-scale atmospheric-oceanic circulations

ENSO acts as one of the most dominant sources in atmosphere-ocean interactions in the tropics, and modulates the climate in extratropical regions through teleconnection [66, 67, 68].

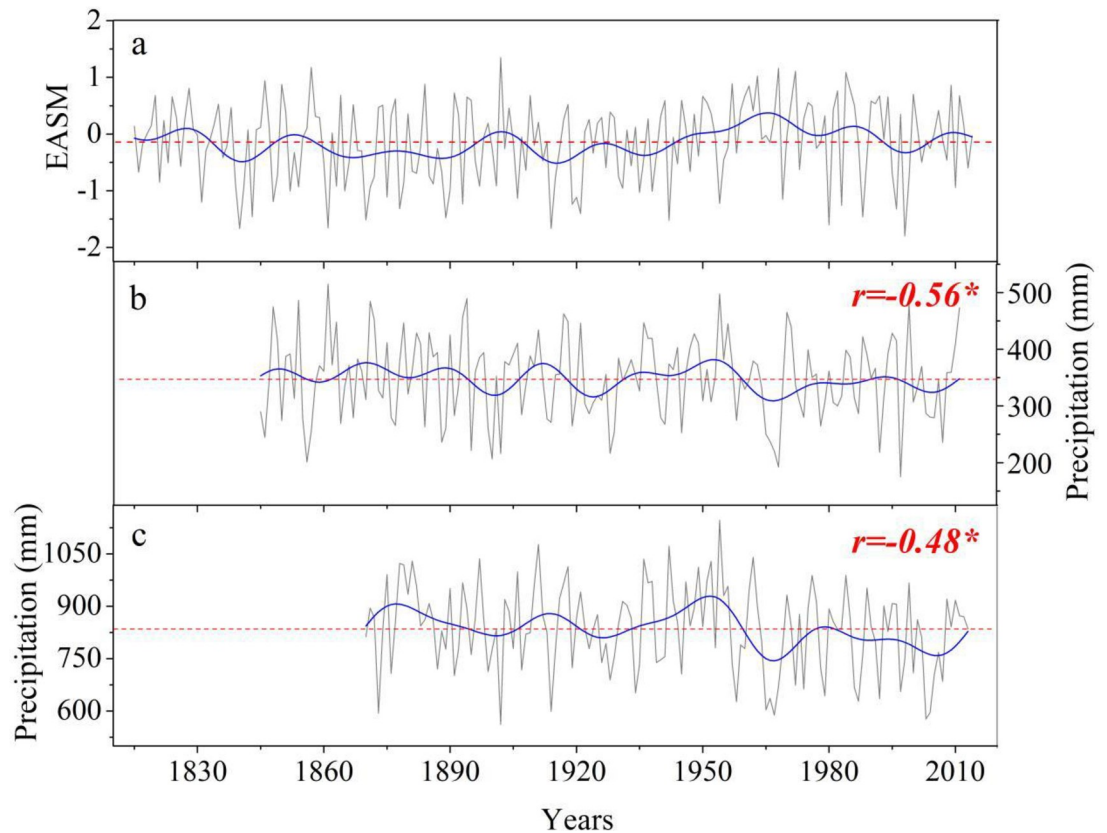


Fig 7. Comparison of (a) the reconstructed EASM with the tree-ring $\delta^{18}\text{O}$ based (b) May-June precipitation reconstruction for BMJ [31] and (c) May-October precipitation reconstruction for AJ [30] over the middle-lower reaches of the Yangtze River. The low-frequency variations isolated by using a 20-year fast-Fourier transform filter are represented by the solid blue lines.

<https://doi.org/10.1371/journal.pone.0234421.g007>

High (low) ENSO variability usually corresponds to strong (weak) ENSO-climate teleconnection [69]. ENSO variance was relatively low during the periods of 1830–1890 and 1930–1960, possibly causing the collapse of the ENSO-EASM teleconnection. When ENSO variance was high, ENSO made significant impacts on EASM changes via modulations of the strength and position of the Western Pacific Subtropical High [70, 71]. Similar interdecadal shifts of ENSO teleconnection have been often highlighted for hydroclimate change over East China and many other regions [28, 29, 67, 68].

Although ENSO still plays an important role for controlling EASM variability, it is worth noting that the strong EASM-ENSO relationship has weakened since 1980s (S6 Fig and Fig 6), raising the possibility that the driving force of EASM dynamics has shifted from natural to anthropogenic in nature [72, 73, 74, 75]. Anthropogenic aerosol emissions in East Asia have increased dramatically since the 1980s because of China's urbanization and industrialization, which can partially mask greenhouse warming and induce strong large-scale atmospheric circulation changes and regional climate responses [72, 73, 74]. Radiative effects due to increased aerosols (especially black carbon) from pollution over the Asian continent could stabilize regional atmospheric convection and hence to reduce the Asia summer monsoon [72, 76, 77, 78]. In addition, the aerosol-induced cooling trend of the upper tropospheric temperature over East Asia also notably modulates the southward shift of the upper-level westerly jet stream and the northward progression of EASM winds without SST-mediated changes, based upon coupled and atmospheric general circulation models [73, 79].

Conclusions

We provided the first EASM reconstruction from 1815 to 2014 using a *P. massoniana* tree-ring cellulose $\delta^{18}\text{O}$ records in the middle Yangtze River basin, a core area of EASM. EASM started to increase with a peak from the 1950s-80s in response to the warming trends. After the 1970s, EASM started to decay, which may correspond to the enhancement of the anthropogenic influences. ENSO is shown to be a critical forcing of EASM variations. However, the EAS-M-ENSO relationships collapsed when the ENSO variance became weak. Despite the high ENSO variance in the 1980s, the ENSO-EASM teleconnection still started to decrease, indicating the overwhelming effect of the anthropogenic factors over natural processes in more recent years.

Supporting information

S1 Fig. Monthly mean temperature (circle), monthly total precipitation (bar) records and monthly mean relative humidity (square) at the Shimen meteorological station as averaged during 1960–2014.

(DOCX)

S2 Fig. The tree-ring standard width chronology of *P. massoniana* (green line) at the study area and the sample replication (gray bar). Dash line denotes the year (1815) with $\text{SSS} > 0.85$.

(DOCX)

S3 Fig. Tree-ring cellulose $\delta^{18}\text{O}$ data of four individual cores from four different trees (WL02, WL19, HP06, HP13) for the period of 1950–2014, respectively.

(DOCX)

S4 Fig. Relationship between June–August total precipitation and average relative humidity for the period of 1960–2014.

(DOCX)

S5 Fig. Wavelet power spectrum of the reconstructed EASM. The thick black contour designates 5% significance level against red noise.

(DOCX)

S6 Fig. Spatial correlations between EASM and precedent winter (from December to February) global SSTs for the period of 1981–2017. Correlations not significant at the 95% level have been masked out. The maps were produced from <https://climexp.knmi.nl>.

(DOCX)

S1 Table. Correlations of the tree-ring cellulose $\delta^{18}\text{O}$ data shown in S3 Fig.

(DOCX)

S2 Table. Documented anomalously flooding events in the middle-lower reaches of Yangtze River with weak EASM detected by tree-ring $\delta^{18}\text{O}$ records. The average value and standard deviation of the reconstructed EASM are -0.12 and 0.71.

(DOCX)

Acknowledgments

The editor and three anonymous reviewers are highly appreciated for their wonderful suggestions and comments, which are really helpful for the improvement of our manuscript.

Author Contributions

Data curation: Zhipeng Dong.

Methodology: Tinghai Ou.

Resources: A'ying Zeng.

Supervision: Keyan Fang.

Writing – original draft: Dai Chen, Feifei Zhou.

References

1. Li J, Cook ER, Chen F, Davi N, D'Arrigo R, Gou X, et al. (2009) Summer monsoon moisture variability over China and Mongolia during the past four centuries. *Geophys Res Lett* 36: 355
2. Shi F, Li J, Wilson R (2014) A tree-ring reconstruction of the South Asian summer monsoon index over the past millennium. *Sci Rep-UK* 4
3. Tao S, & Chen L (1987) A review of recent research on the East Asian summer monsoon in China *Monsoon Meteorology*. Oxford University Press, 60–92
4. Wu R, Wang B (2002) A contrast of the East Asian summer monsoon-ENSO relationship between 1962–77 and 1978–93. *J Climate* 15: 3266–3279
5. Huang R, Chen J, Huang G (2007) Characteristics and variations of the East Asian monsoon system and its impacts on climate disasters in China. *Adv Atmos Sci* 24: 993–1023
6. Zhang P, Cheng H, Edwards RL, Chen F, Wang Y, Yang X, et al. (2008) A test of climate, sun, and culture relationships from an 1810-year Chinese cave record. *Science* 322: 940–942 <https://doi.org/10.1126/science.1163965> PMID: 18988851
7. Cook ER, Anchukaitis KJ, Buckley BM, D'Arrigo RD, Jacoby GC, Wright WE (2010) Asian monsoon failure and megadrought during the last millennium. *Science* 328: 486–489 <https://doi.org/10.1126/science.1185188> PMID: 20413498
8. Wang Y, Cheng H, Edwards RL, Kong X, Shao X, Chen S, et al. (2008) Millennial- and orbital-scale changes in the East Asian monsoon over the past 224,000 years. *Nature* 451:1090–1093 <https://doi.org/10.1038/nature06692> PMID: 18305541
9. Chen F, Xu Q, Chen J, Birks HJB, Liu J, Zhang S, et al. (2015) East Asian summer monsoon precipitation variability since the last deglaciation. *Sci Rep-UK* 11186
10. Wang H (2001) The weakening of the Asian monsoon circulation after the end of 1970's. *Adv Atmos Sci* 18: 376–386
11. Zhou T, Yu R, Li H, Wang B (2008) Ocean forcing to changes in global monsoon precipitation over the recent half century. *J Clim* 21: 3833–3852
12. Xiao J, Xu Q, Nakamura T, Yang X, Liang W, Inouchi Y (2004) Holocene vegetation variation in the Daihai Lake region of north-central China: a direct indication of the Asian monsoon climatic history. *Quaternary Sci Rev* 23: 1669–1679
13. Hong Y, Hong B, Lin Q, Shibata Y, Hirota M, Zhu Y, et al. (2005) Inverse phase oscillations between the East Asian and Indian Ocean summer monsoons during the last 12000 years and paleo-El Niño. *Earth Planet Sc Lett* 231: 337–346
14. Wang Y, Cheng H, Edwards RL, He Y, Kong X, An Z, et al. (2005) The Holocene Asian monsoon: links to solar changes and North Atlantic climate. *Science* 308: 854–857 <https://doi.org/10.1126/science.1106296> PMID: 15879216
15. Fritts HC (1976) *Tree Rings and Climate* Academic, London
16. Cook ER, Kairiukstis LA (1990) *Methods of dendrochronology: applications in the environmental sciences* Springer Science & Business Media
17. Duan J, Zhang Q, Lv L, Zhang C (2012) Regional-scale winter-spring temperature variability and chilling damage dynamics over the past two centuries in southeastern China. *Clim Dynam* 39: 919–928
18. Shi J, Cook ER, Li J, Lu H (2013) Unprecedented January–July warming recorded in a 178-year tree-ring width chronology in the Dabie Mountains, southeastern China. *Palaeogeogr Palaeoecol* 381: 92–97
19. Cai Q, Liu Y, Duan B, Sun C (2018) Regional difference of the start time of the recent warming in Eastern China: prompted by a 165-year temperature record deduced from tree rings in the Dabie Mountains. *Clim Dynam* 50: 2157–2168

20. Wang L, Fang K, Chen D, Dong Z, Zhou F, Li Y (2018) Intensified variability of the El Niño-Southern Oscillation enhances its modulations on tree growths in southeastern China over the past 218 years. *Int J Climatol* 38: 5293–5304
21. Shi J, Lu H, Li J, Shi S, Wu S, Hou X, et al. (2015) Tree-ring based February–April precipitation reconstruction for the lower reaches of the Yangtze River, southeastern China. *Global Planet Change* 131: 82–88
22. Loader N, Robertson I, Barker AC, Switsur VR, Waterhouse JS (1997) An improved technique for the batch processing of small wholewood samples to α -cellulose. *Chem Geol* 136:313–317
23. McCarroll D, Loader N (2004) Stable isotopes in tree rings. *Quat Sci Rev* 23: 771–801
24. Liu X, Wang W, Xu G, Zeng X, Wu G, Zhang X, et al. (2014) Tree growth and intrinsic water-use efficiency of inland riparian forests in northwestern China: evaluation via $\delta^{13}\text{C}$ and $\delta^{18}\text{O}$ analysis of tree rings. *Tree Physiol* 34: 966–980 <https://doi.org/10.1093/treephys/tpu067> PMID: 25145697
25. Roden JS, Ehleringer JR (2000) Hydrogen and oxygen isotope ratios of tree-ring cellulose for riparian trees grown long-term under hydroponically controlled environments. *Oecologia* 121: 467–477
26. Dansgaard W (1964) Stable isotopes in precipitation. *Tellus* 16: 436–468
27. Cai M, Huang Y, Chen M, Liu G, Jin D, Zhou X (2000) A study on hydrogen and oxygen isotopes composition of precipitation in Xiamen. *Journal of Oceanography in Taiwan Strait* 19: 446–453 (in Chinese with English abstract)
28. Sano M, Xu C, Nakatsuka T (2012) A 300-year Vietnam hydroclimate and ENSO variability record reconstructed from tree ring $\delta^{18}\text{O}$. *J Geophys Res Atmos* 117: D12115
29. Xu C, Zheng H, Nakatsuka T, Sano M (2013) Oxygen isotope signatures preserved in tree ring cellulose as a proxy for April–September precipitation in Fujian, the subtropical region of southeast China. *J Geophys Res Atmos* 118: 12, 805–812, 815
30. Xu C, Ge J, Nakatsuka T, Yi L, Zheng H, Sano M (2016) Potential utility of tree ring $\delta^{18}\text{O}$ series for reconstructing precipitation records from the lower reaches of the Yangtze River, southeast China. *J Geophys Res Atmos* 121: 3954–3968
31. Xu C, Shi J, Zhao Y, Nakatsuka T, Sano M, Shi S, et al. (2018) Early summer precipitation in the lower Yangtze River basin for AD 1845–2011 based on tree-ring cellulose oxygen isotopes. *Clim Dynam* 52: 1583–1594
32. Liu Y, Cobb KM, Song H, Li Q, Li C, Nakatsuka T, et al (2017) Recent enhancement of central Pacific El Niño variability relative to last eight centuries. *Nat Commun*, 8
33. Li J, Zeng Q (2002) A unified monsoon index. *Geophys Res Lett* 29: 111–115
34. Trouet V, Van Oldenborgh GJ (2013) KNMI Climate Explorer: a web-based research tool for high-resolution paleoclimatology. *Tree-ring Research* 69: 3–14
35. Rayner N, Parker DE, Horton EB, Folland CK, Alexander LV, Rowell DP, et al. (2003) Global analyses of sea surface temperature, sea ice, and night marine air temperature since the late nineteenth century. *J Geophys Res Atmos* 108: D14
36. Trouet V, Van Oldenborgh G J (2013) KNMI Climate Explorer: a web-based research tool for high-resolution paleoclimatology. *Tree-Ring Research* 69: 3–13
37. Fritts HC (1976) *Tree Rings and Climate*. Academic, London
38. Stokes MA, Smiley TL (1968) *An Introduction to Tree Ring Dating*. The University of Chicago Press, Chicago
39. Holmes RL (1994) *Dendrochronology Program Library (Diskette)* Laboratory of Tree-Ring Research, University of Arizona, Tucson
40. Cook ER (1985) *A time series analysis approach to tree-ring standardization* PhD Thesis, University of Arizona, Tucson
41. Wigley TM, Briffa KR, Jones PD (1984) On the average value of correlated time series, with applications in dendroclimatology and hydrometeorology. *Journal of Climate and Applied Meteorology* 23: 201–213
42. Loader NJ, Robertson I, Barker AC, Switsur VR, Waterhouse JS (1997) An improved technique for the batch processing of small wholewood samples to α -cellulose. *Chem Geol* 136: 313–317
43. Green JW (1963) *Methods in carbohydrate chemistry* In: Whistler RL(eds) *Wood cellulose* Proc 3th Academic Press, New York, p 9–21
44. Yoshimura K, Kanamitsu M, Noone D, Oki T (2008) Historical isotope simulation using reanalysis atmospheric data. *J Geophys Res Atmos* 113 <https://doi.org/10.1029/2007jd009286>
45. Liu X, Shao X, Liang E, Chen T, Qin D, An W, et al. (2009) Climatic significance of tree-ring $\delta^{18}\text{O}$ in the Qilian Mountains, northwestern China and its relationship to atmospheric circulation patterns. *Chem Geol* 268: 147–154.

46. Meko D, Graybill DA (1995) Tree-ring reconstruction of upper Gila Rwer discharge. *Journal of the American Water Resources Association* 31: 605–616.
47. Li J, Xie S, Cook E, Morales MS, Christie DA, Johnson NC, et al. (2013) El Niño modulations over the past seven centuries. *Nature Clim Change* 3: 822–826
48. Vuille M, Werner M, Bradley R, Keimig F (2005) Stable isotopes in precipitation in the Asian monsoon region. *J Geophys Res Atmos* 110: D23108
49. Pyper BJ, Peterman RM (1998) Comparison of methods to account for autocorrelation in correlation analyses of fish data. *Can J Fish Aquat Sci* 55: 2127–2140
50. Li Y, Li J, Feng J (2012) A teleconnection between the reduction of rainfall in southwest Western Australia and north China. *J Climate* 25: 8444–8461
51. Zhou F, Fang K, Li Y, Chen Q, Chen D (2016) Nonlinear characteristics of hydroclimate variability in the mid-latitude Asia over the past seven centuries. *Theor Appl Climatol* 126: 151–159
52. Shi Y, Jiang T, Su B, Chen J, Qin N (2004) Preliminary analysis on the relation between the evolution of heavy floods in the Yangtze River catchment and the climate change since 1840. *Journal of Lake Sciences* 16: 289–297 (in Chinese)
53. Wang M, Zheng H, Xie X, Fan D, Yang S, Zhao Q, et al. (2011) A 600-year flood history in the Yangtze River drainage: comparison between a subaqueous delta and historical records. *Chinese Sci Bull* 56: 188–195
54. Zeng Y, Chen J, Zhu Z, Li J, Wang J, Wan G (2012) The wet little ice age recorded by sediments in huguangyan lake, tropical south china. *Quatern Int* 263.
55. Shi J, Yan Q, Wang H, Jiang D, Min J, Jiang Y (2017) Investigating dynamic mechanisms for synchronous variation of East Asian and Australian summer monsoons over the last millennium. *Palaeogeogr Palaeoclimatol* 480: 70–79.
56. Man W, Zhou T, Jungclaus JH (2012) Simulation of the East Asian summer monsoon during the last millennium with the MPI earth system model. *J Climate* 25: 7852–7866.
57. Dairaku K, Emori S (2006) Dynamic and thermodynamic influences on intensified daily rainfall during the Asian summer monsoon under doubled atmospheric CO_2 conditions. *Geophys Res Lett* 33: 331–330
58. D'Arrigo R, Wilson R, Li J (2006) Increased Eurasian-tropical temperature amplitude difference in recent centuries: Implications for the Asian monsoon *Geophys Res Lett* 33: L22706
59. Sutton RT, Dong B, Gregory JM (2007) Land/sea warming ratio in response to climate change: IPCC AR4 model results and comparison with observations. *Geophys Res Lett* 34: L02701
60. Zhou T, Gong D, Li J, Li B (2009) Detecting and understanding the multi-decadal variability of the East Asian Summer Monsoon-Recent progress and state of affairs. *Meteorol Z* 18: 455–46
61. Liu J, Wang B, Cane MA, Yim SY, Lee JY (2013) Divergent global precipitation changes induced by natural versus anthropogenic forcing. *Nature* 493: 656 <https://doi.org/10.1038/nature11784> PMID: 23364744
62. Menon S, Hansen J, Nazarenko L, Luo Y (2002) Climate effects of black carbon aerosols in China and India. *Science* 297: 2250–2253 <https://doi.org/10.1126/science.1075159> PMID: 12351786
63. Jiang D, Wang H (2005) Natural interdecadal weakening of East Asian summer monsoon in the late 20th century. *Chinese Sci Bull* 50: 1923–1929
64. Fu J, Li S, Luo D (2009) Impact of global SST on decadal shift of East Asian summer climate. *Adv Atmos Sci* 26: 192–201
65. Wang H, Fan K (2013) Recent changes in East Asian monsoon. *Chinese Journal of Atmospheric Sciences* 37: 313–318 (in Chinese with English Abstract)
66. Kumar KK, Rajagopalan B, Cane MA (1999) On the weakening relationship between the Indian monsoon and ENSO. *Science* 284: 2156–2159 <https://doi.org/10.1126/science.284.5423.2156> PMID: 10381876
67. Torrence C, Webster PJ (1999) Interdecadal changes in the ENSO-monsoon system. *J Climate* 12: 2679–2690
68. Mason SJ (2001) El Niño, climate change, and Southern African climate. *Environmetrics* 12: 327–345
69. Li J, Xie S, Cook E, Huang G, D'Arrigo R, Liu F, et al. (2011) Interdecadal modulation of El Niño amplitude during the past millennium. *Nat Clim Change* 1: 114–118
70. Chung PH, Sui CH, Li T (2011) Interannual relationships between the tropical sea surface temperature and summertime subtropical anticyclone over the western North Pacific. *J Geophys Res Atmos* 116: D13111

71. He C, Zhou T, Wu B (2015) The key oceanic regions responsible for the interannual variability of the western North Pacific subtropical high and associated mechanisms. *J Meteorol Res* 29: 562–575
72. Zhao C, Tie X, Lin Y (2006) A possible positive feedback of reduction of precipitation and increase in aerosols over eastern central China. *Geophys Res Lett* 33 <https://doi.org/10.1029/2006gl027800>
73. Liu J, Wang B, Cane MA, Yim SY, Lee JY (2013) Divergent global precipitation changes induced by natural versus anthropogenic forcing. *Nature* 493: 656–659. <https://doi.org/10.1038/nature11784> PMID: 23364744
74. Song F, Zhou T, Qian Y (2014) Responses of East Asian summer monsoon to natural and anthropogenic forcings in the 17 latest CMIP5 models. *Geophys Res Lett* 41: 596–603
75. Fu C (2003) Potential impacts of human-induced land cover change on East Asia monsoon. *Global Planet Change* 37: 219–22
76. Ramanathan V, Crutzen PJ, Mitra AP, Sikka D (2002). The Indian Ocean experiment and the Asian brown cloud. *Current Science* 83: 947–955
77. Bonasoni P, Laj P, Marinoni A, Sprenger M, Angelini F, Arduini J, et al. (2010) Atmospheric Brown Clouds in the Himalayas: first two years of continuous observations at the Nepal Climate Observatory-Pyramid (5079 m). *Atmospheric Chemistry and Physics* 10: 7515–7531
78. Lelieveld J, Bourtsoukidis E, Brühl C, Fischer H, Fuchs H, Harder H, et al. (2018) The South Asian monsoon-pollution pump and purifier. *Science* 361: 270–273 <https://doi.org/10.1126/science.aar2501> PMID: 29903882
79. Wang H, Xie S, Kosaka Y, Liu Q, Du Y (2019) Dynamics of Asian summer monsoon response to anthropogenic aerosol forcing. *J Clim* 32: 843–858